Nanomedicine

The effect of nanoparticle size on *in vivo* pharmacokinetics and cellular interaction

Nanoparticle-based technologies offer exciting new approaches to disease diagnostics and therapeutics. To take advantage of unique properties of nanoscale materials and structures, the size, shape and/or surface chemistry of nanoparticles need to be optimized, allowing their functionalities to be tailored for different biomedical applications. Here we review the effects of nanoparticle size on cellular interaction and *in vivo* pharmacokinetics, including cellular uptake, biodistribution and circulation half-life of nanoparticles. Important features of nanoparticle probes for molecular imaging and modeling of nanoparticle size effects are also discussed.

Nazanin Hoshyar[1], Samantha Gray[1], Hongbin Han[2] & Gang Bao*[1,3]

[1]Department of Biomedical Engineering, Georgia Institute of Technology & Emory University, Atlanta, GA 30332, USA
[2]Department of Radiology, Peking University Third Hospital, Beijing 100191, China
[3]Department of Bioengineering, Rice University, Houston, TX 77030, USA
*Author for correspondence:
Tel.: +1 713 348 2764
Fax: +1 713 348 5877
gang.bao@rice.edu

Over the past 20 years, nanotechnology has become a promising new strategy for disease diagnostics and therapeutics [1,2]. A distinct advantage of nanotechnology is the ability to design and optimize the unique physiochemical properties of nanoscale materials and structures. Altering the size, shape and/or surface chemistry of nanoparticles allows their functionalities to be tailored to meet different requirements [3–5]. Nanoparticles need to reach the targeted organ or tissue in order to realize the desired function. Nanotherapeutics rely on effective cellular uptake and tumor permeability of nanoparticles, which both depend on the size of nanoparticles [1,6–7]. The optimal size of a nanoparticle also depends on the specific location and type of targeted tissue [8]. Rapid clearance of nanoparticles from the blood stream by the mononuclear phagocyte system (MPS) and reticuloendothelial system (RES) is one of the major obstacles to ensuring that nanoparticles can achieve the required accumulation in the target tissue [1,9–10]. Modulation of the pharmacokinetics of nanoparticles to prevent rapid clearance from blood has been achieved by tuning their sizes [9,11], and successful temporary evasion of the RES postinjection has been demonstrated by measuring blood circulation half-life and examining the biodistribution of nanoparticles in the blood, RES organs and targeted tissue [11]. Nanoparticles used to enhance the contrast of an imaging modality also have size-dependent properties. Nanoparticle size influences image contrast, cellular uptake and tumor permeability [12–14]. While the RES can still present an obstacle for required accumulation of nanoparticles, rapid clearance is advantageous for reducing background signal in certain imaging applications [13].

The complexity of finding the optimal nanoparticle size, shape and surface chemistry for a desired use requires additional studies on nanoparticle interactions with cells and tissue [1]. A better understanding nanoparticle size effects on cellular uptake and pharmacokinetics will allow general nanoparticle design rules to emerge [15]. Analytical models may guide the design and functionalization of nanoparticles by providing a quantitative relationship between nanoparticle size

Future Medicine part of fsg

and functionality [15]. The emphasis of this review is placed on the current understanding of the effects of nanoparticle size on cellular uptake and pharmacokinetics, specifically that related to therapeutic and diagnostic applications. Broader reviews on nanoparticles and their applications can be found elsewhere [16–18].

Nanoparticle development

With the growth of nanotechnology and its use in medicine, several methods have been developed to produce highly uniform nanoparticle classes. Here, we explain a few methods currently used to develop nanoparticles. A novel method for coating superparamagnetic iron oxide nanoparticles (SPIOs) was reported by Tong *et al.* They demonstrated that the core size and PEG coating of SPIOs can be tuned to increase the T_2 relaxivity per particle by more than 200-fold [13]. Mackey *et al.* reported on the development of effective gold nanorods for photothermal therapy. They describe a seed mediated growth method to synthesize gold nanorods of approximately 38 nm in length and 11 nm in width. The particles were coating with polyethylene glycol (PEG). A seedless growth method was further described to develop smaller gold nanorods [19]. Liposomes have been used as drug delivery agents and recently used in ultrasound-mediated hyperthermia for cancer therapy [20]. Kheirolomoom *et al.* reported the hydration method used to develop the liposomes followed by Dox loading which created nanoparticles of approximately 100 nm [20,21].

Nanoparticle-cell interactions *in vitro*

There is a growing interest in investigating the effects of nanoparticle size on cellular uptake and targeting [15]. Numerous *in vitro* studies have been conducted, which involve different cell types, probes with various core materials, surface charges and tested size ranges (Table 1) [5,9,12,22–24]. These studies show clear trends of size-dependent behavior in cellular uptake and active targeting.

Cellular uptake

Nanoparticle size, shape and core composition are strong determinants of cellular uptake [1,28]. Creating nanoparticles with a specific shape such as spherical, cubic, rod-like, or worm-like will influences cellular uptake [29,30]. In a comparison between cubic, spherical and rod-like gold nanoparticles, spherical particles showed the highest uptake in terms of weight, but rod-like nanoparticles showed the highest uptake in terms of quantity [30]. DOX-loaded polymeric nanoparticles showed a similar trend, with a higher cellular uptake for rod-like and worm-like nanoparticles than spherical nanoparticles in MCF-7 cells [29].

Nanoparticle size also impacts cellular uptake due to its influence on the enthalpic and entropic properties that govern the adhesion strength between nanoparticles and cellular receptors [4]. Zhang *et al.* developed a thermodynamic model that showed optimal cellular uptake when a ligand-coated nanoparticle is 50 nm in diameter [31]. In experimental studies with HeLa cells, spherical mesoporous silica nanoparticles with a 50-nm diameter showed the highest cellular uptake [22]. In addition, a study using targeted gold nanoparticles reported the highest cellular uptake with 40–50 nm gold nanoparticles in SKBR-3 cells [23]. The same trend was observed when the core was changed from gold to silver [23].

As illustrated in Figure 1, size-dependent uptake via endocytosis of ligand-coated nanoparticles is likely related to the membrane-wrapping process that a nanoparticle undergoes [1,31]. Due to limited number of ligands available, small ligands (antibody, peptide and aptamer) on nanoparticle surface must bind to target proteins (receptors) on the surface of cancer cells in close proximity to drive the membrane-wrapping process. The enthalpic limit for a spherical nanoparticle occurs at a size of about 30 nm, indicating that nanoparticles smaller than this limit will not be able to drive the membrane-wrapping process effectively [32]. The surface of colloidal gold nanoparticles of 2–100 nm were decorated with Herceptin molecules and their cellular uptake were compared with unmodified gold nanoparticles. Significant uptake of Herceptin coated gold nanoparticles were observed in human breast cancer SK-BR-3 cells overexpressing ErbB2 receptor. Receptor mediated uptake is believed to be the mechanism of uptake based on the observation of presence of endosomes and multivesicular bodies [23]. Large nanoparticles drive the membrane-wrapping process by binding to many receptors; however, a nanoparticle above 60 nm in diameter results in a receptor shortage, which decreases uptake because of the increasing entropic penalty [32]. Although the exact optimal diameter varies between applications, a ligand-coated, spherical nanoparticle between 30 and 60 nm in diameter can recruit and bind to enough cellular receptors to drive the membrane-wrapping process without a receptor shortage affecting endocytosis [31,32]. Most *in vitro* studies show a maximum cellular uptake within the 10–60 nm range, regardless of core composition or surface charge [9,12,22,33–34].

There are many other ways nanoparticle can get into cells. For example, nanoparticles can enter a cell through passive penetration [35,36]. Red blood cells (RBCs) are commonly used as in models for passive penetration because RBCs lack endocytic machinery [36]. In a study with both gold and titanium dioxide

Optimal size (nm)	Sizes tested (nm)	ζ-potential (mV)	Nanoparticle type	Cell line	Ref.
Table 1. Summary of studies conducted regarding the effects of nanoparticle size on cellular uptake *in vitro*.					
Nanorods (diameter: height = 1:3)					
30 nm	30, 50, 70, 100		Titanium dioxide	MC3T3-E1	[25]
Spherical nanoparticles					
37 nm	8, 23, 37, 65	12.7 ± 0.75	PVP-coated iron oxide	RAW264.7	[12]
40–50 nm	30, 50, 110, 170, 280		Mesoporous silica	HeLa	[22]
	14, 30, 50, 74, 100		Gold	HeLa	[24]
	16, 24, 40, 58	-39.03 ± 10.42	Gold	RAW264.7 HepG2	[9]
	13, 45, 70, 110	-25.05 ± 4.05	Gold	CL1–0	[26]
	2, 10, 25, 40, 50, 70, 80, 90	-20.04 ± 2.57	Gold	SK-BR-3	[23]
	5, 10, 20, 40, 50, 60, 90	-16.36 ± 0.61	Silver	SK-BR-3	[23]
58 nm	16, 24, 40, 58	28.23 ± 2.59	Gold	RAW264.7 HepG2	[9]
100 nm	30, 40,100	-4.10 ± 3.25	Poly(ethylene glycol)-bl-poly(propylene sulfide	THP-1	[27]
	25, 50, 100, 200, 500	-44.42 ± 4.25	Polystyrene	Caco-2 MDCK	[5]

nanoparticles, passive transport into RBCs was only possible at sizes less than 200 nm, though fewer than one particle per cell was observed [37]. RBCs exposed to silver nanoparticles of 15, 50 and 100-nm diameters exhibited the highest passive uptake of 50 nm particles, averaging more than 45 particles per cell [38].

Other parameters affecting cellular uptake are surface charge and cell type. When comparing the uptake of 2, 4 and 6 nm gold particles in HeLa cells, the ligand coating (cationic, anionic, or zwitterionic) impacted the type of uptake. Zwitterionic particles mainly entered the cell through membrane fusion for sizes less than 6 nm [39]. In contrast, 6 nm zwitterionic particles and all cationic and anionic particles entered the cell through multiple endocytic pathways [39]. Liu *et al.* conducted a study comparing the endocytosis of a range of gold nanoparticle sizes with both positive and negative surface charges [9]. In nonphagocytic HepG2 cells, positively charged nanoparticles showed higher active uptake for each tested size [9]. Interestingly, the positively charged nanoparticles showed the greatest uptake with a 58-nm diameter particle, but the negatively charged nanoparticles showed the greatest uptake with a 40-nm diameter nanoparticle. Based on nanoparticle accumulation in

the secondary lyposomes of HepG2 cells, nanoparticles likely entered via clathrin-mediated endocytosis [9]. Compared to nonphagocytic cells, phagocytic RAW 264.7 cells showed a similar active uptake of positively charged nanoparticles compared with negatively charged nanoparticles. Further comparison of macrophage uptake showed no definitive size-dependent trend in positively charged nanoparticles, but a trend of higher uptake at 40 nm in negatively charged nanoparticles [9]. Nanoparticles formed large aggregates in vacuoles and phagosomes of RAW 264.7 cells, indicating that gold nanoparticles entered the macrophage cells via phagocytosis [9]. Drug-loaded polymeric nanoparticles were tested in a similar manner, and showed similar trends regarding the effects of surface charge. The macrophage cells showed increased uptake with increased nanoparticle size, while nonphagocytic cells showed increased uptake with decreased nanoparticle size [40].

Yu *et al.* explored the size-dependent uptake of macrophage cells alone [27]. Ultrasmall superparamagnetic iron oxide (uSPIOs) nanoparticles surrounded by PEG-poly(propylene sulfide) (PEG-PPS) were synthesized to be 30, 40 and 100 nm in diameter. As previously reported with polymeric nanoparticles,
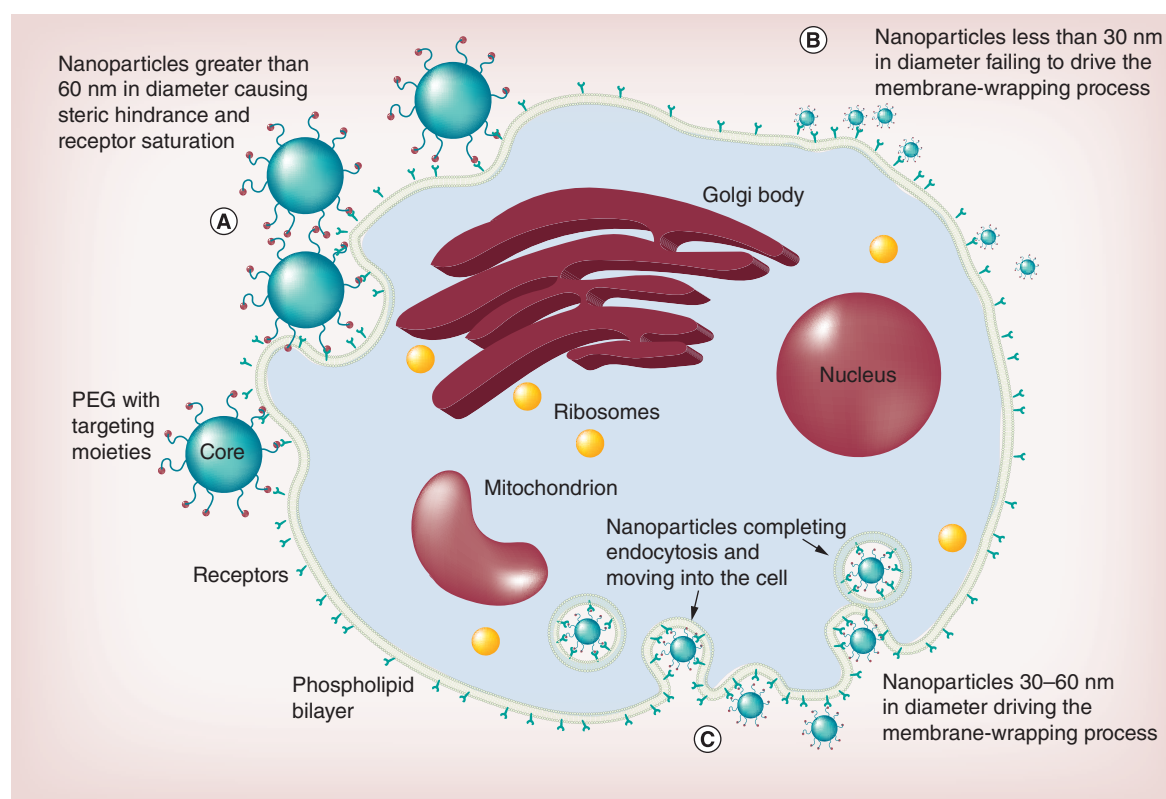
Figure 1. A schematic depicting the effect of nanoparticle size on the membrane-wrapping process.
(A) Nanoparticles greater than 60 nm in diameter driving the membrane-wrapping process by binding to a large number of receptors but limiting the binding of other nanoparticles. **(B)** Nanoparticles less than 30 nm in diameter attaching to some membrane receptors but failing to drive the membrane-wrapping process unless many bind to receptors in close proximity. **(C)** Nanoparticles between 30 and 60 nm in diameter attaching to membrane receptors and driving the membrane-wrapping process effectively.

increased uSPIO size correlated with increased uptake by macrophage cells [27]. However, an *in vitro* study with macrophage cells resulted in the highest uptake at a diameter of 37 nm, which was not the largest size tested [12]. Currently, it is unclear if size-dependent uptake follows a different trend in macrophage cells than in nonphagocytic cells [9,27,40]. To develop a toolbox for designing nanoparticles that avoid the MPS, further studies are required to provide a more complete understanding of the effects of nanoparticle size on macrophage uptake.

Nanoparticle uptake is also dependent on the dose as observed in the result of QD nanoparticles of 4 nm. Various concentration (10, 3 and 1 nM) of QD's were incubated with HeLa cells. A linear decrease of membrane associated fraction of particles were observed with decreasing QD concentration. A critical threshold density of QDs on the cell membrane for very small nanoparticles (4 nm) has to be exceeded to trigger the internalization process. The challenge is to fully understand the dosage effect and there is a need for highly sensitive and sophisticated methods that can analyze the relevant exposure concentrations [41,42].

Active targeting

Nanoparticles are frequently coated with polyethylene glycol (PEG) to avoid the RES system and increase blood circulation half-life. The PEG coating makes the nanoparticle more hydrophilic and neutral, allowing them to bypass the immune system more easily; however, PEG poorly affects the cellular uptake and drug release [11,26,43]. Adding targeting ligands to the surface of a PEG-coated nanoparticle increases cellular uptake, helping to mitigate the uptake loss due to the initial PEG coating. The addition of targeting moieties improves the delivery process through active targeting of overexpressed antigens [44]. Surface ligands that bind to cellular receptors result in receptor-mediated uptake. A critical number of receptor-ligand interactions must occur to produce enough thermodynamic energy to overcome the resistive forces such as membrane elasticity and thermal fluctuations [45]. It is important to note that active targeting has drawbacks. Conjugating certain ligands such as anti-Her2 scFv antibody fragment to pegylated liposomal doxorubicin nanoparticles increases macrophage recognition and allows faster clearance compared with the nontargeted

nanoparticles [26,46]. Active targeting can also create a binding site barrier effect, limiting nanoparticle penetration into the targeted tissue [47]. The *in vivo* drawbacks make it unclear if active targeting actually assists in the delivery process [47].

A possible solution to this problem is masking target ligands with a cleavable PEG-lipid conjugate. Masking the targeting ligands ensures ample circulation time while still utilizing active targeting [48]. In one study, nanoparticles targeted with folate receptor-targeted (FRT) liposomes were masked with acysteine-cleavable 1,2-distearoyl-sn-glycero-3-phosphoethanolamine (DSP)–PEG coating were incubated with 9L glioma cells. Significant uptake was observed only in cells treated with cysteine [48]. Further *in vivo* investigation revealed that the FRT masked nanoparticles did specifically target tumor cells after a cysteine injection and showed higher tumor cell uptake rates than nanoparticles without targeting liposomes, indicating the masking method is a promising solution to difficulties with active targeting [48].

To optimize active targeting via ligand density, Elias *et al.* conducted a study with HER2-targeted superparamagnetic iron oxide nanoparticles (SPIOs) on HER2/neu-positive (T6–17) cells [4]. SPIOs were conjugated to HER2-affibodies previously ligated to an azido-fluorescent peptide (AzFP) at varying concentrations. Twenty-six and 50 nm HER2-AzFP conjugated SPIOs were synthesized with different ligand densities. Both showed that the highest degree of cellular uptake occurs at a concentration of 0.01 ligands/nm squared [4]. The ligand-receptor binding energy also affects cellular uptake. Zhang *et al.* found that a smaller optimal radius and higher maximal cellular uptake is achieved with a larger ligand-receptor binding energy. Within the common range of typical antibody-antigen energies, the optimal radius can range from 25.4 to 30.2 nm [31].

Gold nanoparticles that are targeted to cancer cells show size-dependent cell binding [7]. When comparing 15, 30, 90 and 150 nm targeted gold nanoparticles, the 15-nm diameter nanoparticles showed a 13-fold increase in cellular binding probability compared with the 150-nm diameter nanoparticles. However, 90-nm diameter cells showed optimal targeting in terms of gold mass per cell and surface area per cell [7]. While this indicates an optimal size range, additional studies should be conducted to evaluate the effects of size on targeting with differing parameters (e.g., varying cell lines, nanoparticle shapes and core compositions).

Increasingly sophisticated *in vitro* models will allow for more accurate and realistic testing. Examples of more sophisticated *in vitro* modeling techniques include the simulation of bodily fluids, the agitation of the model system, or the use of multiple cell lines [49]. All of these techniques aim to more closely simulate conditions in the body. Simulating conditions in the body is useful not only for examining aspects of the delivery process, but also for testing nanoparticle responses to changes in the environment such as various pH levels or different enzymatic activity [1]. When conducting any future studies, nanoparticles must be fully characterized so that the fundamental nanoparticle-cell interactions may be understood [22]. The current understanding of the effects of nanoparticle size, summarized above, is useful in designing future studies. For example, future studies regarding active targeting should consider the nanoparticle size since it is already known that optimal ligand density follows a constant trend with increasing nanoparticle size [4]. Well-executed *in vitro* studies will assist in designing successful *in vivo* studies and increasing the understanding of fundamental nanoparticle physicochemical properties, such as size.

In vivo nanoparticle biodistribution & pharmacokinetics

While *in vitro* studies focus on individual aspects of the delivery process, *in vivo* studies shed light on the effects of nanoparticle size within the context of the body. Blood circulation half-life [11,50–52], tumor permeability [6,52–54] and biodistribution [5,11,50,55–56] are all affected by the size of the nanoparticle. Table 2 provides a summary of several *in vivo* studies showing size-dependent trends.

Blood circulation half-life

Once a foreign object enters a body, opsonization begins. Opsonin proteins attach to the foreign object and make it more visible to the mononuclear phagocytic system (MPS) [58]. A rapid MPS response results in the clearance of uncoated nanoparticles from the bloodstream within a few hours postinjection [5,9,50]. The rapid clearance of nanoparticles limits their use because nanoparticles do not have time to reach the targeted tissue [59]. Problems with avoiding the MPS have moved nanoparticles from the first generation of material design and biocompatibility to the second generation of stealth tactics and active targeting [1]. While some advances have increased circulation half-life ($t_{1/2}$), such as PEG coating [3,11,26,43], a closer look at the basic size of a nanoparticle shows significant, size-dependent changes in $t_{1/2}$. Blood circulation half-life is typically measured by injecting the nanoparticles and detecting the concentration of nanoparticles in the blood at certain time points. To evaluate the blood circulation half-life of [60] Cu-mSPIOs, 10 mg Fe/kg of radiolabeled nanoparticles were injected via mouse tail vein. The animals were

Table 2. Summary of *in vivo* studies conducted with spherical nanoparticles that focus on the effects of nanoparticle size directly.

Core material	Animal model	Coating	Core sizes (nm)	$t_{1/2}$ (h)	Ref.
Gold	BALB/c mice	PEG$_{5000}$	5.3	48.9	[50]
		PEG$_{5000}$	21.6	31.8	
		PEG$_{4000}$	41.2	13.8	
		PEG$_{5000}$	51.4	13.7	
		PEG$_{7000}$	58.1	11.4	
		PEG$_{10,000}$	76.5	8.7	
		PEG$_{20,000}$	98.3	6.8	
Gold	CD1 mice	PEG$_{2000}$	17.72	4.0	[52]
		PEG$_{2000}$	31.28	2.4	
		PEG$_{2000}$	45.03	0.4	
		PEG$_{2000}$	66.54	1.0	
		PEG$_{5000}$	17.72	29.7	
		PEG$_{5000}$	31.28	19.3	
		PEG$_{5000}$	45.03	14.1	
		PEG$_{5000}$	66.54	9.2	
		PEG$_{5000}$	86.73	3.3	
		PEG$_{10,000}$	17.72	51.1	
		PEG$_{10,000}$	31.28	27.7	
		PEG$_{10,000}$	45.03	16.1	
		PEG$_{10,000}$	66.54	11.3	
		PEG$_{10,000}$	86.73	6.6	
Gold	CD1 mice	PEG$_{2000}$	16.6	2.5	[52]
		PEG$_{2000}$	22.6	4.0	
		PEG$_{5000}$	32.5	16.5	
		PEG$_{10,000}$	43.3	11.6	
		PEG$_{10,000}$	83.5	7.2	
Quantum dots	SCID mouse bearing an Mu89 human melanoma	PIL-coated	10.7	24.7	[57]
		Silica shell and PEG$_{5000}$	56.7	16.6	
		Silica shell and PEG$_{5000}$	122.4	9.70	

sacrificed and blood was collected at 10 min, 1 h, 4 h and 24 h postinjection. The circulation half-life of [60] Cu-mSPIOs was found to be 143 ± 21 min [61].

Some specific size limitations are known. Some classes of nanoparticle with a diameter less than approximately 10 nm will be rapidly eliminated by the kidneys [11,62]. To facilitate the rapid renal clearance of small molecules drugs, the renal filtration barrier, has an effective size cutoff of ≈10 nm [62]. Clearance of nanoparticles is typically measured by labeling them with a fluorescence dye or radiotracer (such as [60] Cu), and quantifying the amount of nanoparticles in the excreted urine for clearance [10].

The reason for this clearance can be found by looking at each component of the kidney's filtration system. The kidney uses peritubular capillaries and renal corpuscles to filter the blood and produce urine. Within a renal corpuscle is the glomerulus, which has three layers with varying pore sizes. The effective size cutoff of the overall structure is 10 nm [50]. The upper size limit of nanoparticles can vary based on the targeted cellular receptors [63], but a nanoparticle with a diameter greater than 200 nm will activate the complement system and be quickly removed from the blood stream, accumulating in the liver and spleen [3,5,51]. Moghimi *et al.* suggest a maximum size

limit of 150 nm for spherical nanoparticles to avoid filtration in the spleen [55].

Further studies have narrowed the range of sizes and provided additional information about the effects of size on $t_{1/2}$. In a comparison between 24 and 37 nm shell cross-linked nanoparticles, the smaller particle had a higher retention at 10 min and at 4 h postinjection. At 1 h postinjection, 50% of the smaller nanoparticles were found in circulation, compared with only 5% of the larger nanoparticles [59]. A study with gold nanoparticles systematically tested the effects of nanoparticle size and mPEG weight on $t_{1/2}$. Five different nanoparticles, ranging from 17.72 to 86.73 nm, were each coated with mPEG 2 kDa, 5 kDa and 10 kDa. The nanoparticles were injected into CD-1 mice, and $t_{1/2}$ was calculated from blood samples drawn at specific time intervals. For each size, $t_{1/2}$ increases as mPEG molecular weight increases. The greatest change is seen from mPEG 2 kDa to mPEG 5 kDa [52]. Between various core sizes, the smaller nanoparticles have a longer $t_{1/2}$. For example, there was an eightfold increase in $t_{1/2}$ from the 86 nm core to the 17 nm core with the same coating [52]. Therefore, decreasing nanoparticle size and increasing the molecular weight of the PEG coating increases $t_{1/2}$ [11,52]. A visual depiction of the trends between nanoparticle size and $t_{1/2}$ is shown in Figure 2, including the material, coating and charge of the tested particles.

Biodistribution

To fully understand a nanoparticle's pharmacology, it is important to extensively analyze toxicology, pharmacokinetic and efficacy testing in preclinical models. Quantitative biodistribution can be performed to estimate the total number of nanoparticles in the entire body at a given time point after injection or exposure. Regardless of nanoparticles route of administration (inhalation, gavage to the GI tract, intravenous injection or by dermal applications), distribution of nanoparticles in organs and tissues of interest can be assessed. After administration, particle distribution is measured at several time points after using suitable methods. Nonradioactive nanoparticles can be quantified in the collected specimens using analytical chemistry (e.g., inductively coupled plasma mass spectroscopy or atomic absorption mass spectroscopy) [64–66].

Biodistribution changes depending on nanoparticle properties and interactions with the living system [15]. In particular, nanoparticle size affects the biodistribution of nanoparticles throughout the body [11,50–51,56]. Particles on the micrometer scale remain in the body much longer than particles on the nanometer scale [51]. In one *in vivo* mouse model, micrometer particles remained in the spleen and the site of injection for at least two weeks, while nanoparticles of the same material were almost completely cleared in the same time frame [51]. The largest accumulations of nanoparticles typically occur in the blood, liver and spleen [11]. Generally, larger nanoparticles accumulate in the liver and spleen more rapidly. There is still debate as to whether the rapid accumulation is due to simple filtration or increased binding opportunities between the MPS cells and the nanoparticles [58]. In a study comparing 10, 40, 150 and 10,000 nm Al_2O_3 nanoparticles, a significantly lower percentage of the injected dose of the 10 nm nanoparticles accumulated in the liver compared with all larger nanoparticles [60]. A higher accumulation of the 10 nm nanoparticles was observed in the kidneys, but this could be caused by a lessened availability of the larger nanoparticles due to their high accumulations in the liver. Biodistribution data for Al_2O_3 particles can be seen in Figure 3A. Examining the variations in biodistribution for 24 and 37-nm diameter shell cross-linked nanoparticles, smaller particles show a lower accumulation in the liver at 10 min postinjection and lower kidney uptake at 4 h postinjection. Uptake in the spleen showed no correlation to nanoparticle size [59].

The minimum size to escape renal filtration, 10 nm, is illustrated by examining the biodistribution of spherical gold nanoparticles with diameters of 10, 50, 100 and 250 nm at 24 h postinjection. The 50-nm diameter nanoparticle shows the lowest accumulation in both organs, but the 10-nm diameter nanoparticle shows the highest accumulation in the spleen and the liver [11]. In contrast, 15, 50 and 160 nm gold nanoparticles functionalized with PEG show decreasing accumulation from 50 to 15 nm [67]. In a study by Sonavane *et al.*, the biodistribution of various sized gold nanoparticles (15, 50, 100 and 200 nm) were observed in mice. Their results showed that smaller particle size gold nanoparticles like 15 and 50 nm had higher blood concentration 24 h postadministration. Organ biodistribution studies also showed that 15 nm gold nanoparticles had a wide spread concentration compared with larger sizes. Increase in spleen concentration was observed with the increase in particle size [56].

Nanoparticle size impacts biodistribution within specific organs, as well as affecting the biodistribution throughout the body. The size-dependent distribution of nanoparticles is the result of various filters within organs or barriers between the organ and the surrounding fluid [5,50]. For example, when nanoparticles from 20 to 100 nm in diameter were injected into the kidney tissue, no correlation between the particle size and particle accumulation was found in the peritubular capillaries. However, there was a strong correlation between particle size and particle accumulation in the renal cor-
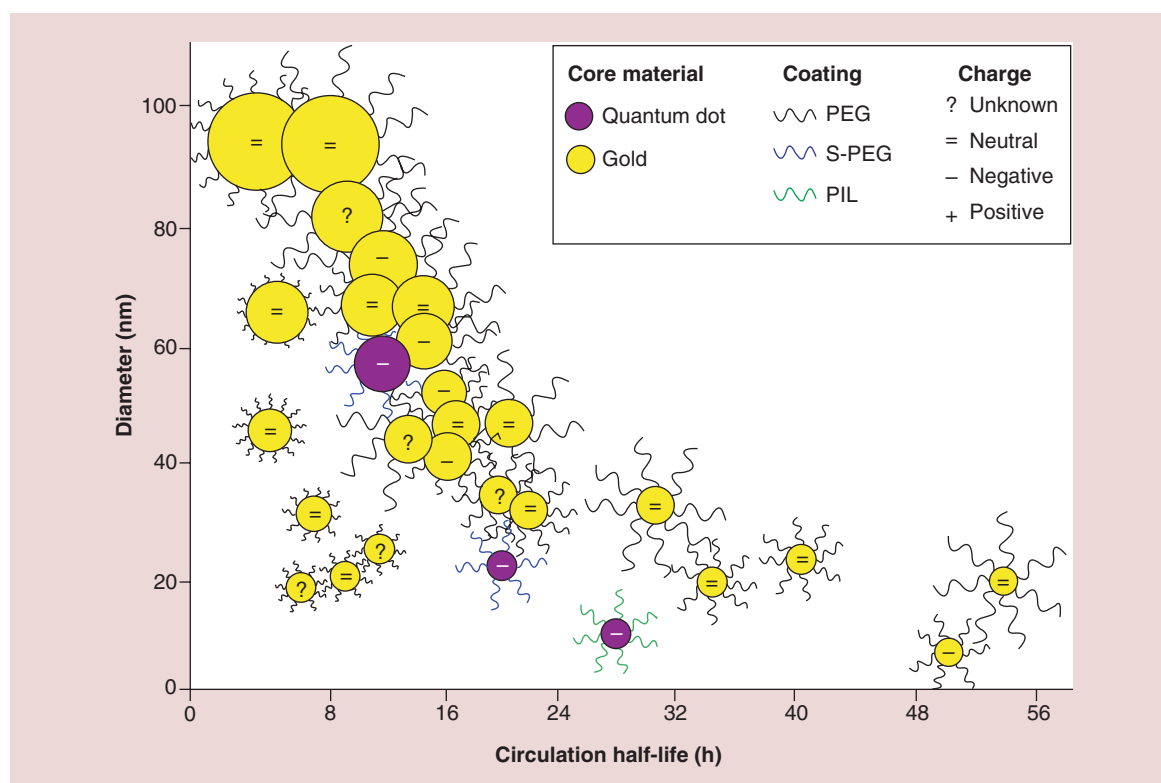
Figure 2. A schematic representing the relationship between nanoparticle size and circulation half-life. Each point represents a specific combination of characteristics that has been tested. Points are colored based on core material (yellow represents gold and purple represents quantum dots). The coating of the particle is shown by the lines surrounding each point. Black lines denote a PEG coating, with longer lines representing higher PEG molecular weight. Blue lines denote an S-PEG coating (silica shell with PEG_{5000} coating). Green lines denote a PIL coating. Within each point, surface charge is shown as positive (+), negative (-), neutral (=), or unknown (?).

puscles. Nanoparticles 50 nm in diameter accumulated in all renal corpuscle cells with decreasing quantities as the nanoparticle diameter approaches the extremes of the tested range [50]. An example of a barrier's impact can be found in a study that analyzed the effects of size when penetrating the blood–brain barrier. Polystyrene nanoparticles between 25 and 500 nm were injected into rats; 3 h postinjection, the biodistribution of nanoparticles showed a strong correlation to nanoparticle size (Figure 3B). Notably, 25 and 50 nm particles showing the greatest accumulation in the brain tissue [5]. A similar trend appeared in the study of gold nanoparticles mentioned above by Sonavane *et. al.* The gold concentration of 15 and 50 nm nanoparticles in the brain revealed that the smaller sized particles are able to pass the blood–brain barrier [56].

It is interesting to note that certain nanoparticles do not have traditional pharmacokinetic profile and biodistribution. Liposomes can be modified to alter the PK/PD profile [68]. Geiser *et al.* reviewed the biokinetics and clearance of nanoparticles deposited in the respiratory tract. They compared the nanometer sized particles with micrometer sized particles in

the 0.5–10 µm range [65]. Experimental studies have shown that the accumulation and translocation of some nanoparticles such as inhaled iridium particles in secondary target organs depends on particle size [64]. Biodistribution of 1.4 and 18 nm gold nanoparticles after their intratracheal instillation also showed that significant difference exist in their translocation and accumulation [69].

In order to determine the effects of nanoparticle size on biodistribution, nanoparticle properties and biodistribution model parameter must be quantified [15]. A possible future method of evaluating the biodistribution of nanoparticles is a physiologically based pharmacokinetic model (PBPK) [15,70]. PBPK models are discussed in further detail in the modeling section.

Tumor permeability

Although nanoparticles can be tailored to reach the targeted tumor, challenges still exist in delivering them to the tumor cells. When a tumor is developing, angiogenesis occurs to supply the rapidly dividing cells with blood and nutrients. These new blood vessels show much higher levels of vascular endothelial growth fac-

tor-A (VEGF-A) than most adult tissue. VEGF-A, a protein highly expressed in healing tissue and developing tissues, is the main protein that helps to drive pathological angiogenesis [71,72]. VEGF increases the vascular permeability of the endothelial cell layer, resulting in 'leaky' blood vessels that create the phenomena known as the enhanced permeability and retention (EPR) effect [71,73]. Vascular permeability depends on both nanoparticle and pore size. As nanoparticle size increases, the vascular permeability decreases [54]. The pore size of tumor vesicles varies based on tumor type and growth location. For example, tumors in the cranial window have dramatically smaller pore sizes than the same tumors in the dorsal chamber [8]. Therefore, nanoparticle size should be tailored depending on the type and location of the tumor.

The 'leaky' blood vessels result in higher interstitial fluid pressure (IFP) within the tumor [6]. This elevated IFP hinders the transport of nanoparticles across the vessel walls and compromise the benefits of the EPR effect [54]. A possible solution to this transport challenge is the normalization of the tumor interstitial matrix [54]. For each nanoparticle size, an ideal pore size exists that maximizes transvascular flux [74]. Chauhan *et al.* simulated the effects nanoparticles from 1 to 250 nm with various mean pore size to evaluate the possible benefits of normalization. Therapeutics under 12 nm showed the most rapid tumor penetration rates [6]. Tumor penetration rates decrease with larger particles. For diffusive and convective penetration in the transvascular and interstitial, smaller particles showed faster penetration [6]. Each nanoparticle size showed an individual optimal mean pore size for maximum delivery. Pore sizes over 140 nm hindered delivery because of the IFP. Experimentation with fluorescently labeled quantum dots of 12, 60 and 125-nm diameter showed higher tumor penetration with smaller particles. The 12 nm particles diffused away from the vessel with minimal hindrance, but 60 nm particles remained within 10 μm of the vessel walls. The 125 nm particles did not extravasate [57]. The same trend was seen with gold nanoparticles [75]. In summary, smaller pore sizes and nanoparticle sizes are preferable for drug delivery [6,75].

When designing a nanoparticle to target a tumor cell, there must be a balance between circulation half-life and the ability to reach the tumor. Generally, a nanoparticle less than 50 nm protected by a moderate mPEG weight seems to have a long half-life and the ability to extravasate into and permeate through the tumor [52]. With any nanoparticle in the 40–100 nm range, circulation half-life is crucial to tumor accumulation. Since nanoparticles move from the blood to the tumor by a concentration gradient through the EPR

effect, a greater concentration in the blood will speed this process [52].

Once nanoparticles accumulate in the tumor, their distribution throughout tumor mass is hindered by the hydrostatic pressure, particularly in the center of the tumor [52,55]. The high central pressure creates a mass-flow movement of fluid away from the center of the tumor, making it difficult for nanoparticles to reach the innermost areas [55]. Subsequent hypoxia, a lack of oxygen to the center of the tumor, often leads to metastasis [57]. Nanoparticles that reach the center of the tumor have slowed and restricted movement through the tumor cell extracellular matrix (ECM) in a size-dependent manner [52]. A possible solution to this problem is using targeting ligands to enhance uptake [76]. However, this creates a binding site barrier that slows the tumor penetration. Currently, it is known that an increased circulation half-life will allow for increased penetration, but the specific nanoparticle size that allows for effective drug delivery capabilities and eliminates the binding site barrier effect still needs to be found [76].

A study of radiolabeled iron oxide nanoparticles on mice bearing human breast cancer tumors compared nanoparticles between 20 and 100 nm diameters. Inductively heating the nanoparticle caused tumor necrosis. The slowed tumor growth for the 20-nm diameter particles was significantly higher than the untreated group or any larger sized particles, despite the increased heat capacity of 30–100-nm diameter particles [53]. Several studies have shown that the size of the nanoparticle significantly affects tumor penetration and favors nanoparticles less than 30 nm in diameter [6,53].

Immunological issues

The ability to manipulate a nanoparticle's size, shape and surface charge allows nanoparticles to be used in many types of immune-regulation. Most notably, nanoparticles have the potential to be a vaccine carrier. Already, nanoparticles conjugated to vaccine antigens have shown higher uptake rates than microsized particles [77]. Nanoparticles between 25 and 40 nm also penetrate tissue well, aiding in the activation of adaptive immune responses [77]. Vaccines may target dendritic cells (DCs) or antigen-presenting cells (APCs). Nanoparticles greater than 500 nm are mainly internalized at the injection site by APCs, while nanoparticles below 200 nm are mainly internalized by DCs [78].

Nanoparticles are being developed as antigen-carriers to avoid antibody production against the platform [30]. A variety of gold nanoparticles were tested for immunogenicity. Tested particles included 20 and 40 nm spherical nanoparticles, 40 × 40 × 40 nm cubic nanopar-
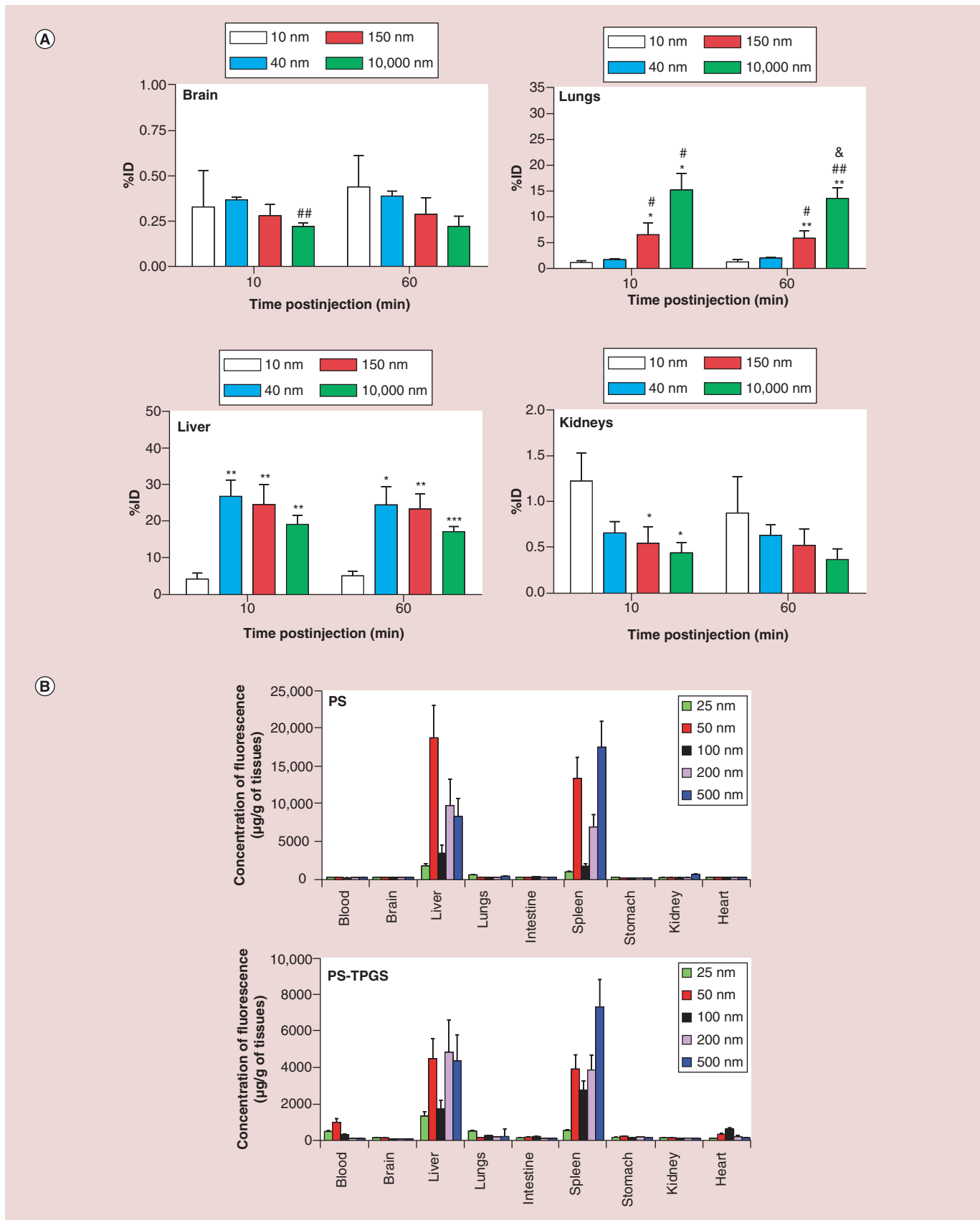
Ⓐ

Ⓑ

Figure 3. Biodistribution of nanoparticles showing the effect of size (please see facing page). (A) Biodistribution of ^{13}N-labeled Al_2O_3 nanoparticles in male rats 60 min postinjection. Graphs show percent injected dose that has accumulated in the brain (top left), liver (bottom left), lungs (top right) and kidneys (bottom right). Reproduced with permission from [60]. **(B)** Biodistribution of bare and TPGS coated fluorescent polystyrene nanoparticles (PS NPs) in Sprague–Dawley rats 3 h postinjection.
Reproduced with permission from [5].

ticles, and 40 × 10 nm nanorods. Comparing spherical, cubic and rod nanoparticles, the rod shape showed the most efficient uptake by APCs. However, 40 nm spherical nanoparticles were the best platform because they included the secretion of proinflammatory cytokines [30]. Nanoparticle size also impacts T cell response, and this response varies based on the type of T cell. $CD4^+$ T cells show a higher proliferation with larger nanoparticles (>100 nm) [79,80]. However, particles 40–50 nm have stronger $CD8^+$ T cell responses [78].

In addition to vaccine uses, nanoparticles are useful in cell tracking. Since immune cells respond to environmental factors, monitoring immune cells *in vivo* would provide insight into optimal delivery routes, therapeutic doses, etc. [81]. Labeling cells with iron oxide nanoparticles and then performing an MRI gives high-resolution images of the deep tissues [81]. Immune cells can be labeled through *ex vivo* incubation, through *in situ* nanoparticle injection, or *in vivo* systematic application [81].

Many small-scale *in vivo* studies have been conducted, but these independent studies are often difficult to compare because of experimental variations (e.g., different cell lines, different core materials and different nanoparticle coatings). A greater number of large-scale *in vivo* studies would allow direct side-by-side comparisons, elucidating the effects of a single nanoparticle property more easily [11]. For example, studies regarding tumor permeability need to be conducted on a wide range of tumor models and tumor growth stages in order for the trends to be generalized [52]. Furthermore, delivering therapeutics to a tumor is one of the most popular applications of nanoparticles, and there are many aspects of the delivery process that are not understood. Future research in this process needs to be conducted, with an emphasis on the variability of the tumor's extracellular matrix and the permeability of various nanoparticle sizes [52]. These studies must consider the impact of nanoparticle size, summarized above, as well as fundamental concepts shown in relevant *in vitro* studies.

Nanoparticle probes for molecular imaging
MRI
Nanotechnology has touched on major imaging modalities with a variety of radiolabeled nanoparticles. Of these imaging modalities, PET/MR imaging shows the greatest potential for clinical use since MRI soft tissue contrast is combined with PET sensitivity [3–4,53]. MR imaging contrast is determined by the longitudinal relaxation rate $(1/T_1)$ and transverse relaxation rate $(1/T_2)$ [82]. Contrast agents can alter these relaxation rates. The quantitative relaxation rate change normalized by the contrast agent concentration is known as relaxivity [12,82]. Contrast agents that predominantly affect the longitudinal relaxivity (r_1) create positive contrast, increasing signal intensity, while those that predominantly affect the transverse relaxivity (r_2) create negative contrast [12,14,82].

To date, iron oxide nanoparticles are the most widely used MRI contrast agent because of their contrast-enhancing capabilities, biocompatibility and high r_2 relaxivity [4,12–13,53]. The r_2 relaxivity, also known as T_2 relaxivity, of iron oxide nanoparticles increases with increasing particle size, which causes an increase in negative contrast [12,14]. Huang *et al.* reported r_2 relaxivity of PVP-coated iron oxide nanoparticles ranging from 173.37 mM [-1] s [-1] to 248.89 mM [-1] s [-1] for cores ranging from 8 to 65 nm, respectively [12]. These are significantly higher r_2 relaxivity values than Feridex, a well-known MRI contrast agent. Furthermore, the PVP-coated iron oxide nanoparticles with a 37-nm diameter (PVP-IO-37) had the greatest cellular uptake (1.3, 2.8 and 5.3 times the uptake of nanoparticles of size 65, 23 and 8 nm, respectively) *in vitro* and an r_2 relaxivity of 239.98 mM [-1]s [-1]. When comparing PVP-IO-37 to Feridex and nanoparticles of sizes 8, 23 and 65 nm, PVP-IO-37 showed a significantly higher negative contrast enhancement *in vivo* [12]. From these results, it is evident that both r_2 relaxivity and cellular uptake must be considered when choosing a contrast agent.

In addition to size-dependent r_2 relaxivity, superparamagnetic iron oxide nanoparticles show a clear correlation between nanoparticle size and r_1 relaxivity [14]. A study tested nanoparticles between 3.2 and 7.5 nm and found a linear increase in r_1 relaxivity with increasing particle size (seen in Figure 4A) [14]. However, particle size more strongly affects r_2 relaxivity, resulting in a direct relationship between r_2/r_1 relaxivity ratio and particle size [14]. Therefore, smaller particles make better positive contrast agents while larger particles make better negative contrast agents.

The surface coating of the nanoparticle also affects MR imaging contrast. For example, PEG chain length affects T_2 relaxivity [77]. Tong *et al.* tested two different iron oxide core sizes, each coated with five different
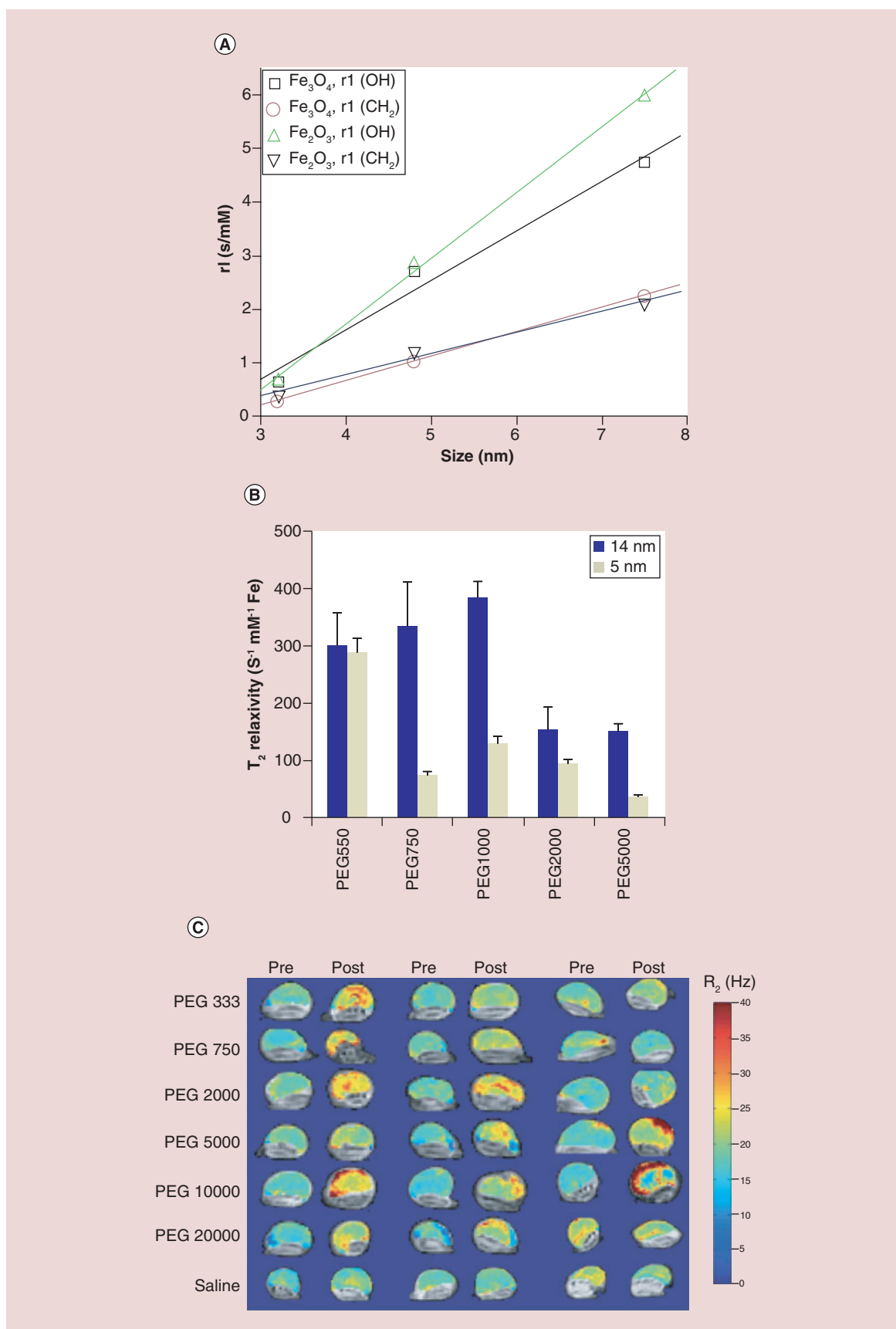
Figure 4. Size-dependent relaxivities of nanoparticle probes. (A) r_1 relaxivity for magnetite in various oxidation states. Each shows a positive, linear correlation between nanoparticle size and r_1 relaxivity. Reprinted with permission from [14]. **(B)** T_2 relaxivity of the SPIOs on a per particle basis. SPIOs with two core sizes, 5 and 14 nm, and five PEG sizes, molecular weight of 550, 750, 1000, 2000 and 5000 Da, were evaluated. Reproduced with permission from [13]. **(C)** MRI images before (pre) and after (post) magnetic nanoparticle injection into the foot on the hind leg of mice with a subcutaneous SCCVII tumor. A 3T scanner was used. Reproduced with permission from [83].

PEG chain lengths, that resulted in the T_2 relaxivity values seen in Figure 4B [13]. As expected, the 14 nm core showed a higher T_2 relaxivity than the 5 nm core with the same PEG coating. However, both core sizes showed an optimal PEG chain length that was not the maximum length. For the 14 nm core, T_2 relaxivity increased by 2.54-fold with a decrease in PEG molecular weight from 5000 to 1000 Da and then did not continue to increase as the PEG molecular weight further decreased. Likewise, 5 nm cores showed a critical PEG size of 550 Da [13]. *In vivo* testing of the optimally-PEG-coated 14 nm core particles revealed significant MRI contrast [13]. Various PEG molecular weight coatings can also impact distribution of particles across a target, as seen in the tumor scans in Figure 4C. Smaller PEG molecular weights provide a more even spread across the target. As the PEG molecular weight increases, particles tend to accumulate along the rim of the target [83]. Another consideration is ligand density, which impacts negative contrast in MR imaging. The optimal density of 0.01 ligands/nm squared provides a significant improvement in contrast compared with both higher and lower ligand densities [4]. Since optimal ligand density is size-dependent, researchers must consider the size of the nanoparticle when conjugating ligands to the surface of imaging probes [4].

Luminescence imaging

When imaging *in vitro*, nanoparticles can be used to increase image contrast and sensitivity [84]. One way of utilizing nanoparticles is through dye-doping, or modulation to absorb a specific dye. When using dye-doped nanoparticles, size is critical because it determines both the luminescence and intracellular mobility [84]. In a study with dye-doped silica nanoparticles, a 23 nm nanoparticle was compared with 85 nm particles in regards to penetration time and retention. Nanoparticle penetration was comparable for both sizes during the first 20 min of incubation. After 40 min of incubation, the 23 nm nanoparticles had penetrated the cell membrane in 58% of cells, while 85 nm nanoparticles had penetrated only 14% of cells. The size of the nanoparticles also affected the location, with 23 nm nanoparticles retained evenly throughout the cytosol, illuminating the entire cell, and 85 nm nanoparticles retained along the outer cell surface, forming a luminous ring [84].

A second method uses the luminescence of noble metal nanoparticles, such as gold [85]. Differing optical properties such as plasmon absorption can be modulated through size [86]. In a study of silica-gold nanospheres and gold nanorods, Jain *et al.* found that the optical resonance wavelength, the extinction cross-section, and the relative contribution of scattering to the extinction, are strongly dependent on the nanoparticle dimensions. It was observed that an increase in size correlated to an increase in extinction and relative scattering contribution [85]. Overall, more work is needed to fully understand the effect of size on optical properties of nanoparticles and optimize them for *in vitro* luminescence imaging.

Magnetic particle imaging

Magnetic particle imaging (MPI) is a new topographic imaging technique that focuses solely on the distribution of superparamagnetic iron oxide nanoparticles in biological tissue, providing high sensitivity, spatial resolution, and contrast [87,88]. It can be used in cancer targeting, vascular imaging, and stem cell labeling and tracking [87]. MPI relies heavily on nanoparticle size because superparamagnetism only occurs in ferromagnetic particles that are smaller than a critical diameter [88]. MPI involves measuring particle magnetization under a static magnetic field. For superparamagnetic iron oxide nanoparticles, the magnetization is nonlinear and produces harmonics [88]. The MPI images created by analyzing these harmonics depend on nanoparticle relaxation times of the magnetic moments, referred to as MPI tracers, in the presence of an oscillating magnetic field. Relaxation times increase with the increasing diameter for Neél relaxation time, Brownian rotational diffusion, and hysteretic reversal [88]. The effects of MPI tracer size are substantial, even in the small range of 7–22 nm [87]. Additionally, the effectiveness of MPI tracers is affected by the environment, so size can be tuned to the preferred application [87].

The main areas of research within diagnostic imaging involve enhancing current techniques. Nanoparticles have already shown an ability to increase imaging contrast in MR and *in vitro* imaging [53]. Future imaging improvements involving nanoparticles could range from contrast agents that can be detected by multiple imaging modalities to dual-modality imaging probes that combine radionuclide-based and non-radionuclide-based imaging approaches [53]. Prospective research also involves recent imaging techniques specifically focused on nanoparticles, such as MPI. Models for MPI have shown promise, but research is

needed to see the actual effects of various nanoparticle properties. In both areas of research, nanoparticle size affects imaging. This occurs through varying T_2 relaxivity measurements, luminescence levels, Néel relaxation, Brownian rotational diffusion, and hysteretic reversal mechanisms [13,53,88]. Future studies must not only consider nanoparticle size in the experimental design, but also fully characterize nanoparticles so that researchers can make fair comparisons and learn more about the effects of nanoparticle size on imaging.

Modeling of nanoparticle size effects

The growing interest in understanding the movements, cellular internalization and excretion of nanoparticles with different sizes, core materials and surface modifications has led to the development of various models. A range of thermodynamic based and physiologic based pharmacokinetic models have been developed to begin the task of organizing and interpreting the wide range of experimental data [15,31,70].

Thermodynamic models

The thermodynamic interaction between a nanoparticle and the cell membrane, a critical step in delivery, depends on the nanoparticle's physiochemical factors [89]. In one particular model, the ability of nanoparticles to absorb through the membrane and surround themselves with a layer of phospholipids from the cell membrane is represented by a series of density functions. While only shown with a small range of results (1–4 nm), the trend showed that the larger nanoparticles were able to absorb into the membrane more effectively [89]. A thermodynamic model focusing on cellular uptake of ligand-coated nanoparticles is based on the idea of a thermodynamic equilibrium at which a certain number of nanoparticles undergo endocytosis. Parameters for the model were developed based on the experimental data. The model predicted an optimal radius of 25 nm to maximize cellular uptake [31]. These two model demonstrate the various applications of thermodynamic modeling and allow the prediction of the interactions between nanoparticles and the cell membrane [31,89].

Physiologically based pharmacokinetic models

Physiologically based pharmacokinetic (PBPK) models have been used for the past 30 years to predict and analyze toxicity, absorption, distribution, metabolism and excretion (ADME) of small molecules [15]. The same type of model can be adapted to nanoparticles in an attempt to understand the general rules for designing and implementing of such particles. Since size and surface chemistry strongly affect biodistribution, optimizing these characteristics will improve accumulation the targeted tissue. PBPK models consider the ability

of the nanoparticle to circulate (perfusion) and to penetrate into tissue (permeability) [70]. PBPK models are normally divided into two groups based these transport mechanisms: perfusion (or blood flow) limited and permeability (or membrane) limited [70]. A diagram of these two models is shown in Figure 5A. Within these two categories, PBPK models can also be divided into perfusion and permeability by organ [15].

Once a model is chosen based on the type of nanoparticle and disease state the pharmacokinetic (PK) parameters are established from prior experimentation. These PK parameters are utilized in the model's primary equations and simulations to determine the bioavailability (F), estimated blood circulation half-life ($t_{1/2}$) and excretion of the newly designed nanoparticle [15,70].

With so many different nanoparticle types, the model parameters can vary. For example, poly(lactic-co-glycolic) acid (PLGA) nanoparticles have significantly different diffusion and partition coefficients than those of PEG containing PLGA nanoparticles [70]. When simulating the half-life of four different sized nanoparticles containing PEG and having a zeta potential of -5.26±0.79 mV, both permeability and perfusion models were used. The simulated perfusion model worked more efficiently for nanoparticles that have a shorter $t_{1/2}$, but the simulations from the permeability model more closely aligned with the *in vivo* $t_{1/2}$ results for all nanoparticles [70].

To predict the development of tumor microvasculature, a computational model was developed. This two-dimensional model accounted for tumor-growth and adhesion of nanoparticles to the blood vessel wall. Nanoparticle size, ligand density and vascular receptor expression levels believed to affect the nanoparticle vascular affinity. It was also shown that nanoparticles bypass the tumor mass through the health vessels when the new vasculature network is not sufficiently developed [91].

To model the delivery of FITC-dextran nanoparticle, Anne L van de Ven *et al.* reported the use of IVM (intravital microscopy). The degree of nanoparticle accumulation inside tumor microvasculature was used to understand tumor specific differences. The data suggest that tumor heterogeneity among different individual will lead to variation in tumor response. Without relying on PK models, this method could be used to rank and classify tumors and ultimately understand nanoparticle behavior in preclinical setting [92]. Wu *et al.*, further investigated the effect of interstitial pressure and lymphatic vascular system by modeling these effects and building on the tumor growth model. Interstitial fluid pressure during vascularized tumor growth was found to hinder nanoparticle extravasation [93,94]. To predict the behavior of intravenously injected nanovectors, Godin *et al.* reported a multiscale, multiphysics mathematical model
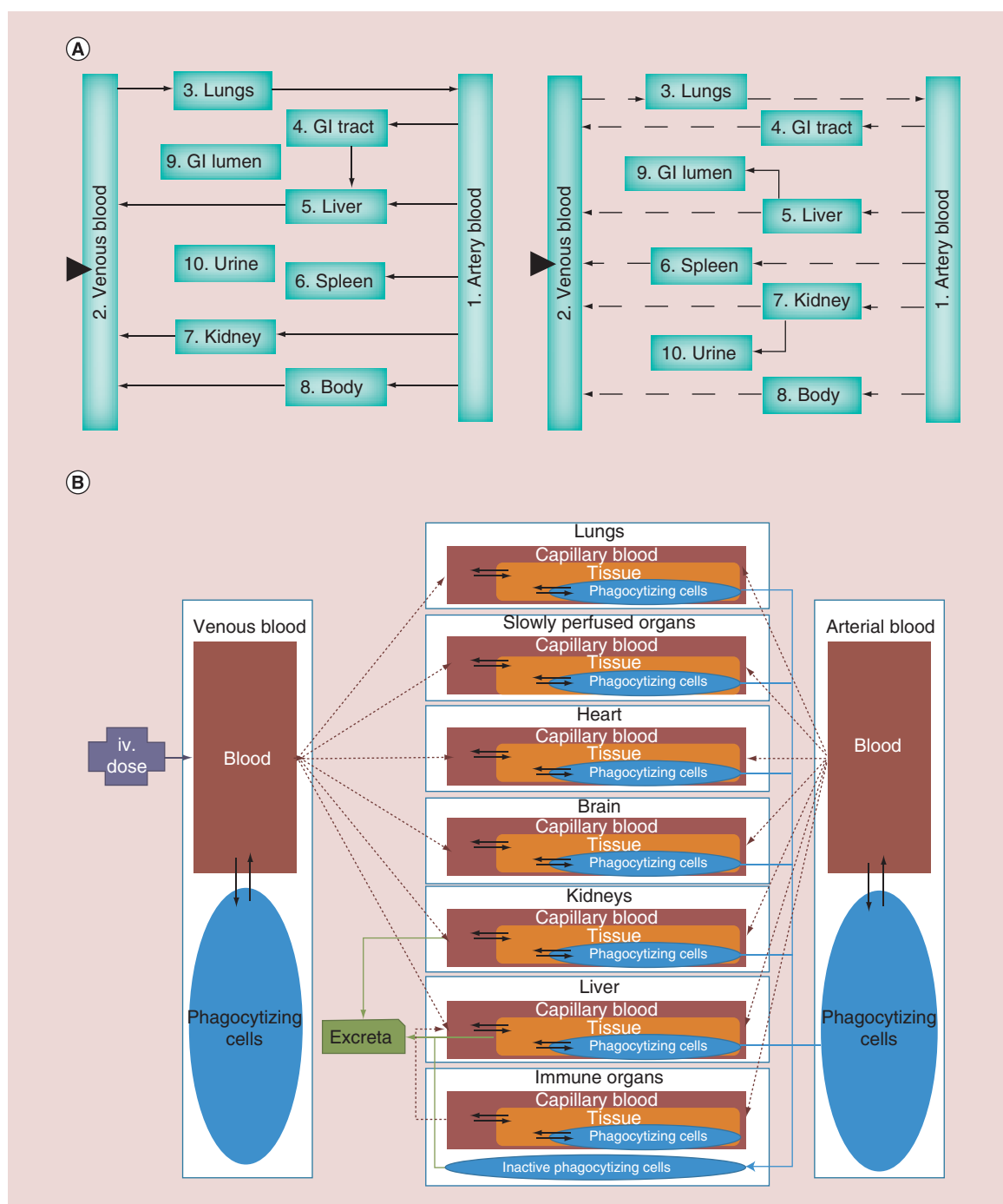
Figure 5. Schematics of PBPK models for nanoparticle permeability. (A) A perfusion model (left) and permeability model (right) with the solid triangle indicating intravenous injection, arrows indicating nanoparticle transportation direction and dashed arrows indicating transportation equations in the permeability model that differ from those in the perfusion model. **(B)** A schematic of a more complex permeability model that considers the effects of phagocytosis on nanoparticle distribution.
(A) Reproduced with permission from [70].
(B) Reproduced with permission from [90].
iv.: Intravenous.

which combined three modules. To model the convective and diffusive transport of nanovectors within the vascular network, a boundary value problem was described. The second module, presented the margination and adhesion dynamic of a single nanovector in close proximity of vessel wall. In addition of to external

forces, effect of nanovector size, shape and specific/non-specific interaction were taken into account. The third module, explored the cellular internalization of nano-vectors with the prior knowledge that the rate of uptake is affected by the geometry and surface physiochemi-cal properties of nanovectors. Design maps were then generated with the integration of the above-mentioned modules. To maximize the localization of nanovectors within diseased microvasculature, the maps may be uti-lized in the identification of optimum combination of size, shape and surface properties [95].

These base models showed promising results, but the complexity of the variances within nanoparticle properties has led to a need for more complex PBPK models which take into consideration the nanopar-ticle type, disease state and nanospecific phenomena in the body [15,70,90]. One model examined the effects of phagocytosis on nanoparticle biodistribution (sche-matic shown in Figure 5B). The model was adapted to several nanoparticle types, and in each case it was found that increased size correlates with increased phagocytiz-ing cell uptake [90]. The more relationships discovered between nanoparticle characteristics and the human body, the more accurate models can become. Currently, the complexity of nanoparticle properties is the lack of data available to use for PK parameter estimations in simulating PBPK models. Nonetheless, PBPK modeling is still a viable option for initial screenings and refine-ment of nanoparticles for their use as therapeutic and diagnostic tools in future research studies.

Conclusion & future perspective

Nanoparticle size significantly influences their thera-peutic and diagnostic applications. Therapeutic deliv-ery aspects, including blood circulation half-life [3,51], targeting [4,7] cellular uptake [12,31] and tumor pen-etration [1,6,51] are all influenced by nanoparticle size. While an optimal size can be determined based on the therapeutic goals, disease site and other nanoparticle properties, some key components can be generalized to all purposes [15,31,70,88]. Nanoparticles must be larger than 10 nm to avoid the renal filtration barrier [3,62]. A diameter greater than 200 nm will activate the comple-ment system and be quickly removed from the blood stream, accumulating in the liver and spleen [3,5,51]. Within this range, a diameter of about 50 nm shows the greatest cellular uptake in thermodynamic mod-els and most experimental studies [12,23,31]. Conversely, nanoparticles 20 nm or less show the greatest tumor penetration [1,6,53]. With these contradictory findings and the constant battle against rapid clearance to RES organs, the 'ideal' nanoparticle is still to be discovered. In fact, it is likely that the optimal nanoparticle design will be disease-specific [57].

Diagnostic imaging shows improved contrast and sensitivity when coupled with nanoparticles [3,88]. MR imaging contrast depends on T2 relaxation time, which is directly related to iron oxide nanoparticle core diame-ter. Likewise, MPI imaging shows increased Neél relax-ation time, Brownian rotational diffusion and hysteretic reversal with an increased core diameter [88]. Once cellu-lar uptake is considered, a core diameter of 37 nm shows the most promise in MRI [12]. In addition to the core diameter, coating must be carefully considered when choosing an MRI contrast agent. An optimal PEG coat-ing length exists for each nanoparticle size [13]. *In vitro* luminescence imaging shows size-dependent trends for gold nanoparticles, with an increased diameter corre-lating to an increased extinction and relative scattering contribution [85]. For dye-doped nanoparticles used in *in vitro* imaging, the cellular uptake and intracellular mobility of the nanoparticles strongly affects the image. A smaller diameter of 23 nm results in improved cellular uptake and moves further past the outer cell membrane to disperse in the cytoplasm than a larger diameter of 85 nm for silica dye-doped nanoparticles [81].

With the variety of therapeutic and diagnostic appli-cations, different nanoparticle sizes are needed, depend-ing on the desired goal. To streamline the construction of new nanoparticles, both thermodynamic models [31,89] and PBPK models [15,70,90] are being developed and fine-tuned. These models account for the nanoparticle's size, surface chemistry and shape [15,70,90]. With advances in understanding the effect of nanoparticle size on interac-tions with the human body, both through models and experimentation, researchers are moving towards imple-menting nanoparticles as a standard in clinical diagnos-tic imaging and drug delivery. Nanoparticles have the potential to be extremely effective therapeutic and diag-nostic tools in a variety of applications. Using nanopar-ticles in the medical field would result in lower systemic doses, enhanced therapeutic efficacy, less unwanted side effects, easier drug administration, increased patient quality of life and compliance [5]. To advance nanopar-ticles into clinical research, further research is needed to elucidate the interaction between the nanoparticles and the human body.

Executive summary

Effects of nanoparticle size: *in vitro* applications
- Nanoparticle size impacts the enthalpic and entropic properties that govern the interaction between nanoparticles and living cells.
- Most *in vitro* studies show a maximum cellular uptake in nonphagocytic cells within the size range of 10–60 nm, regardless of nanoparticle core composition or surface charge.
- The addition of targeting moieties may improve the delivery efficiency through active targeting of overexpressed antigens.
- Within the range of typical antibody-antigen energies, a nanoparticle's optimal radius can range from 25.4 to 30.2 nm.
- Well-executed *in vitro* studies will help generate knowledge of fundamental nanoparticle physicochemical properties, such as the effects of nanoparticle size.

Effects of nanoparticle size: *in vivo* applications
- Some nanoparticles with a diameter less than ~10 nm may be rapidly eliminated by the kidneys.
- A nanoparticle with a diameter greater than 200 nm may activate the complement system and be quickly removed from the blood stream.
- Optimizing nanoparticle size and the molecular weight of the PEG coating increases circulation half-life.
- The largest accumulation of nanoparticles typically occurs in the blood, liver and spleen, with larger nanoparticles accumulating in the liver and spleen more rapidly.
- The size-dependent distribution of nanoparticles within organs is a result of various filters or barriers between the organ and the surrounding fluid.
- As nanoparticle size increases, vascular permeability decreases.
- For each nanoparticle size, an ideal pore size exists that maximizes transvascular flux.
- A greater number of large-scale *in vivo* studies would allow direct side-by-side comparisons, facilitating the elucidation of the effects of individual nanoparticle properties.

Imaging
- In general, the T_2 relaxivity of iron oxide nanoparticles increases with core size, both at constant iron concentration and on a per particle basis.
- Magnetic particle imaging (MPI) is a new topographic imaging technique that focuses solely on the distribution of superparamagnetic iron oxide nanoparticles in biological tissue, providing high sensitivity, spatial resolution and contrast.
- The effects of MPI tracer size are substantial, even in the small range of 7–22 nm.

Modeling
- Thermodynamic models of the effect of nanoparticle size focus on the energy considerations, especially the interactions between nanoparticles and their environment (including cells).
- Physiologically based pharmacokinetic (PBPK) models can be used to perform theoretical analysis and parametric simulations to determine the bioavailability, blood circulation half-life and excretion of nanoparticles.
- The complexity of the variations with nanoparticle properties has led to a need for more complex models that take into account the nanoparticle size and surface chemistry, particle-tissue interaction and other nanospecific phenomena in the body.

References

Papers of special note have been highlighted as:
- of interest; •• of considerable interest

1   Albanese A, Tang PS, Chan WCW. The effect of nanoparticle size, shape, and surface chemistry on biological systems. *Ann. Rev. Biomed. Eng.* 14, 1–16 (2012).

2   Mitragotri S Anderson DG, Chen X *et al.* Accelerating the translation of nanomaterials in biomedicine. *ACS Nano* 9, 6644–6654 (2015).

3   de Barros AB, Tsourkas A, Saboury B, Cardoso VN, Alavi A. Emerging role of radiolabeled nanoparticles as an effective diagnostic technique. *EJNMMI Res.* 2, 39–53 (2012).

4   Elias DR, Poloukhtine A, Popik V, Tsourkas A. Effect of ligand density, receptor density, and nanoparticle size on cell targeting. *Nanomedicine* 9, 194–201 (2013).

5   Kulkarni SA, Feng SS. Effects of particle size and surface modification on cellular uptake and biodistribution of polymeric nanoparticles for drug delivery. *Pharmaceut. Res.* 30, 2512–2522 (2013).

6   Chauhan VP, Stylianopoulos T, Martin JD *et al.* Normalization of tumour blood vessels improves the delivery of nanomedicines in a size-dependent manner. *Nat. Nanotechnol.* 7, 383–388 (2012).

7   Peretz V, Motiei M, Sukenik CN, Popovtzer R. The effect of nanoparticle size on cellular binding probability. *J. Atom. Mol. Opt. Phys.* 2012, 1–7 (2012).

8   Hobbs SK, Monsky WL, Yuan F *et al.* Regulation of transport pathways in tumor vessels: role of tumor type and microenvironment. *Proc. Natl Acad. Sci. USA* 95, 4607–4612 (1998).

9   Liu X, Huang N, Li H, Jin Q, Ji J. Surface and size effects on cell interaction of gold nanoparticles with both phagocytic and nonphagocytic cells. *Langmuir* 29, 9138–9148 (2013).

10   Choi HS, AUTHOR AUTHOR *et al.* Renal clearance of quantum dots. *Nat. Biotechnol.* 25, 1165–1170 (2007).

11   Dreaden EC, Austin LA, Mackey MA, El-Sayed MA. Size matters: gold nanoparticles in targeted cancer drug delivery. *Therapeut. Deliv.* 3, 457–478 (2012).

••   **Gives details of the effects of size in cellular uptake, imaging and drug delivery using gold nanoparticles.**

12   Huang J, Bu L, Xie J *et al.* Effects of nanoparticle size on cellular uptake and liver MRI with polyvinylpyrrolidone-coated iron oxide nanoparticles. *ACS Nano* 4, 7151–7160 (2010).

13   Tong S, Hou S, Zheng Z, Zhou J, Bao G. Coating optimization of superparamagnetic iron oxide nanoparticles for high T2 relaxivity. *Nano Lett.* 10, 4607–4613 (2010).

14   Kucheryavy P, He J, John VT *et al.* Superparamagnetic iron oxide nanoparticles with variable size and an iron oxidation state as prospective imaging agents. *Langmuir* 29, 710–716 (2013).

••   **Details the effects of nanoparticle size on both r_1 and r_2 relaxivities and discusses the subsequent effect on imaging contrast.**

15   Li M, Al-Jamal KT, Kostarelos K, Reineke J. Physiologically based pharmacokinetic modeling of nanoparticles. *ACS Nano* 4, 6303–6317 (2010).

16   Kim BYS, Rutka JT, Chan WCW. Nanomedicine. *N. Engl. J. Med.* 363, 2434–2443 (2010).

17   Bao G, Mitragotri S, Tong S. Multifunctional nanoparticles for drug delivery and molecular imaging. *Annu. Rev. Biomed. Eng.* 15, 253–282 (2013).

18   Torchilin VP. Multifunctional, stimuli-sensitive nanoparticulate systems for drug delivery. *Nat. Rev. Drug Discov.* 13, 813–827 (2014).

19   Mackey MA, Ali MRK, Austin LA, Near RD, El-Sayed MA. The most effective gold nanorod size for plasmonic photothermal therapy: theory and *in vitro* experiments. *J. Phys. Chem. B* 118, 1319–1326 (2014).

20   Kheirolomoom A, Lai CY, Tam SM *et al.* Complete regression of local cancer using temperature-sensitive liposomes combined with ultrasound-mediated hyperthermia. *J. Control. Release* 172, 266–273 (2013).

21   Kheirolomoom A, Mahakian LM, Lai CY *et al.* Copper-doxorubicin as a nanoparticle cargo retains efficacy with minimal toxicity. *Mol. Pharm.* 7, 1948–1958 (2010).

22   Lu F, Wu SH, Hung Y, Mou CY. Size effect on cell uptake in well-suspended, uniform mesoporous silica nanoparticles. *Small* 5, 1408–1413 (2009).

23   Jiang W, Kim BYS, Rutka JT, Chan WCW. Nanoparticle-mediated cellular response is size-dependent. *Nat. Nanotechnol.* 3, 145–150 (2008).

24   Chithrani BD, Ghazani AA, Chan WCW. Determining the size and shape dependence of gold nanoparticle uptake into mammalian cells. *Nano Lett.* 6, 662–668 (2006).

25   Brammer KS, Oh S, Cobb CJ, Bjursten LM, van der Heyde H, Jin S. Improved bone-forming functionality on diameter-controlled TiO(2) nanotube surface. *Acta Biomaterialia* 5, 3215–3223 (2009).

26   Wang M, Thanou, M. Targeting nanoparticles to cancer. *Pharmacolog. Res.* 62, 90–99 (2010).

27   Yu SS, Lau CM, Thomas SN *et al.* Size- and charge-dependent non-specific uptake of PEGylated nanoparticles by macrophages. *Int. J. Nanomedicine* 7, 799–813 (2012).

28   Zhang S, Gao H, Bao G. Physical principles of nanoparticle cellular endocytosis. *ACS Nano* 9(9), 8655–8671 (2015).

29   Karagoz B, AUTHOR AUTHOR *et al.* Polymerization-induced self assembly (PISA) – control over the morphology of nanoparticles for drug delivery applications. *Polym. Chem.* 5, 350–355 (2014).

30   Niikura K, Matsunaga T, Suzuki T *et al.* Gold nanoparticles as a vaccine platform: influence of size and shape on immunological responses *in vitro* and *in vivo*. *ACS Nano* 7, 3926–3938 (2013).

31   Zhang S, Li J, Lykotrafitis G, Bao G, Suresh, S. Size-dependent endocytosis of nanoparticles. *Adv. Mater.* 21, 419–424 (2009).

32   Yuan H, Li J, Bao G, Zhang, S. Variable nanoparticle-cell adhesion strength regulates cellular uptake. *Phys. Rev. Lett.* 105, 138101 (2010).

•   **Shows the effects of size on the membrane-wrapping process based on enthalpic and entropic limits.**

33   Wang SH, Lee CW, Chiou A, Wei PK. Size-dependent endocytosis of gold nanoparticles studied by three-dimensional mapping of plasmonic scattering images. *J. Nanobiotechnol.* 8, 33 (2010).

34   Cruje C, Chithrani BD. Integration of peptides for enhanced uptake of PEGylayed gold nanoparticles. *J. Nanosci. Nanotechnol.* 15, 2125–2131 (2015).

35   Shang L, Nienhaus K, Nienhaus GU. Engineered nanoparticles interacting with cells: size matters. *J. Nanobiotechnol.* 12 (2014).

36   Wang T, Bai J, Jiang X, Nienhaus GU. Cellular uptake of nanoparticles by membrane penetration: a study combining confocal microscopy with FTIR spectroelectrochemistry. *ACS Nano* 6, 1251–1259 (2012).

37   Rothen-Rutishauser B, Schurch S, Haenni B, Kapp N, Gehr P. Interaction of fine particles and nanoparticles with red blood cells visualized with advanced microscopic techniques. *Environ. Sci. Technol.* 40, 4353–4359 (2006).

38   Chen LQ, Fang L, Ling J, Ding CZ, Kang B, Huang CZ. Nanotoxicity of silver nanoparticles to red blood cells: size dependent adsorption, uptake, and hemolytic activity. *Chem. Res. Toxicol.* 28, 501–509 (2015).

39   Jiang Y, Huo S, Mizuhara T *et al.* The interplay of size and surface functionality on the cellular uptake of sub-10 nm gold nanoparticles. *ACS Nano* 9(10), 9986–9993 (2015).

40   He C, Hu Y, Yin L, Tang C, Yin, C. Effects of particle size and surface charge on cellular uptake and biodistribution of polymeric nanoparticles. *Biomaterials* 31, 3657–3666 (2010).

41   Jiang X, Röcker C, Hafner M, Brandholt S, Dörlich RM, Nienhaus GU. Endo- and exocytosis of zwitterionic quantum dot nanoparticles by live HeLa cells. *ACS Nano* 4, 6787–6797 (2010).

42   Treuel L, Jiang X, Nienhaus GU. New views on cellular uptake and trafficking of manufactured nanoparticles. *J. R. Soc. Interface* 10, 20120939 (2013).

43   Ruiz A, Salas G, Calero M *et al.* Short-chain PEG molecules strongly bound to magnetic nanoparticle for MRI long circulating agents. *Acta Biomaterialia* 9, 6421–6430 (2013).

44   Salvati A, Pitek AS, Monopoli MP *et al.* Transferrin-functionalized nanoparticles lose their targeting capabilities when a biomolecule corona adsorbs on the surface. *Nat. Nanotechnol.* 8, 137–143 (2013).

45   Nel AE, Mädler L, Velegol D *et al.* Understanding biophysicochemical interactions atthe nano–bio interface. *Nat. Mater.* 8, 543–557 (2009).

46   Shmeeda H, Tzemach D, Mak L, Gabizon, A. Her2-targeted pegylated liposomal doxorubicin: retention of target-specific binding and cytotoxicity after *in vivo* passage. *J. Control. Release* 136, 155–160 (2009).

47   Lee H, Fonge H, Hoang B, Reilly RM, Allen, C. The effects of particle size and molecular targeting on the intratumoral and subcellular distribution of polymeric nanoparticles. *Mol. Pharmaceut.* 7, 1195–1208 (2010).

48   McNeeley KM, Karathanasis E, Annapragada AV, Bellamkonda RV. Masking and triggered unmasking of targeting ligands on nanocarriers to improve drug delivery to brain tumors. *Biomaterials* 30, 3986–3995 (2009).

49   Gamboa JM, Leong KW. *In vitro* and *in vivo* models for the study of oral delivery of nanoparticles. *Adv. Drug Deliv. Rev.* 65, 800–810 (2013).

50   Choi CHJ, Zuckerman JE, Webster P, Davis ME. Targeting kidney mesangium by nanoparticles of defined size. *Proc. Natl Acad. Sci. USA* 108, 6656–6661 (2011).

51   Faraji AH, Wipf, P. Nanoparticles in cellular drug delivery. *Bioorg. Med. Chem.* 17, 2950–2962 (2009).

52   Perrault SD, Walkey C, Jennings T, Fischer HC, Chan WCW. Mediating tumor targeting efficiency of nanoparticles through design. *Nano Lett.* 9, 1909–1915 (2009).

53   Hong H, Zhang Y, Sun J, Cai W. Molecular imaging and therapy of cancer with radiolabeled nanoparticles. *Nano Today* 4, 339–413 (2009).

54   Jain RK, Stylianopoulos T. Delivering nanomedicine to solid tumors. *Nat. Rev. Clin. Oncol.* 7, 653–664 (2010).

•   **Drug delivery to tumors is the most common therapeutic goal, and this article gives background on the challenges, information on the current state and ideas for the future.**

55   Moghimi SM, Hunter AC, Andresen TL. Factors controlling nanoparticle pharmacokinetics: an integrated analysis and perspective. *Ann. Rev. Pharmacol. Toxicol.* 52, 481–503 (2012).

56   Sonavane G, Tomoda K, Makino, K. Biodistribution of colloidal gold nanoparticles after intravenous administration: effect of particle size. *Colloids Surf. B Biointerfaces* 66, 274–280 (2008).

57   Popović Z, Liu W, Chauhan VP *et al.* A nanoparticle size series for *in vivo* fluorescence imaging. *Angew. Chem. Int. Ed. Engl.* 49, 8649–8652 (2010).

58   Owens DE III, Peppas NA. Opsonization, biodistribution, and pharmacokinetics of polymeric nanoparticles. *Int. J. Pharmaceut.* 307, 93–102 (2006).

59   Sun X, Rossin R, Turner JL *et al.* An assessment of the effects of shell crosslinked nanoparticle size, core composition, and surface PEGylation on *in vivo* biodistribution. *Biomacromolecules* 6, 2541–2554 (2005).

60   Pérez-Campaña C, Gómez-Vallejo V, Puigivila M *et al.* Biodistribution of different sized nanoparticles assessed by positron emission tomography: a general strategy for direct activation of metal oxide particles. *ACS Nano* 7, 3498–3505 (2013).

61   Glaus C, Rossin R, Welch MJ, Bao G. *In vivo* evaluation of (^{64})Cu-labeled magnetic nanoparticles as a dual-modality PET/MR imaging agent. *Bioconjug. Chem.* 21, 715–722 (2010).

62   Zuckerman JE, Choi CHJ, Han H, Davis ME. Polycation-siRNA nanoparticles can disassemble at the kidney glomerular basement membrane. *Proc. Natl Acad. Sci. USA* 109, 3137–3142 (2012).

63   Bartlett DW, Davis ME. Physicochemical and biological characterization of targeted, nucleic acid-containing nanoparticles. *Bioconjug. Chem.* 18, 456–468 (2007).

64   Kreyling WG, Semmler M, Erbe F *et al.* Translocation of ultrafine insoluble iridium particles from lung epithelium to extrapulmonary organs is size dependent but very low. *J. Toxicol. Environ. Health* 65(20), 1513–1530 (2002).

65   Geiser M, Kreyling WG. Deposition and biokinetics of inhaled nanoparticles. *Part. Fibre Toxicol.* 7, 1–17 (2010).

66   Semmler M, Seitz J, Erbe F *et al.* Long-term clearance kinetics of inhaled ultrafine insoluble iridium particles from the rat lung, including transient translocation into secondary organs. *Inhal. Toxicol.* 16(6–7), 453–459 (2004).

67   Terentyuk GS, Maslyakova GN, Suleymanova LV *et al.* Circulation and distribution of gold nanoparticles and induced alterations of tissue morphology at intravenous particle delivery. *J. Biophotonics* 2, 292–302 (2009).

68   Liu Y, Rohrs J, Wang P. Advances and challenges in the use of nanoparticles to optimize PK/PD interactions of combined anti-cancer therapies. *Curr. Drug Metab.* 15, 818–828 (2014).

69   Semmler-Behnke M, Kreyling WG, Lipka J *et al.* Biodistribution of 1.4 nm and 18 nm gold particles in rats. *Small* 4(12), 2108–2111 (2008).

70   Li M, Panagi Z, Avgoustakis K, Reineke J. Physiologically based pharmacokinetic modeling of PLGA nanoparticles with varied mPEG content. *Int. J. Nanomedicine* 7, 1345–1356 (2012).

71   Carmeliet P, Jain RK. Molecular mechanisms and clinical applications of angiogenesis. *Nature* 473, 298–307 (2011).

72   Nagy JA, Dvorak AM, Dvorak HF. VEGF-A and the induction of pathological angiogenesis. *Annu. Rev. Pathol. Mech. Dis.* 2, 251–275 (2007).

73   Fang J, Nakamura H, Maeda, H. The EPR effect: unique features of tumor blood vessels for drug delivery, factors

involved, and limitations and augmentation of the effect. *Adv. Drug Deliv. Rev.* 63, 136–151 (2011).

74   Stylianopoulos T, Soteriou K, Fukumura D, Jain RK. Cationic nanoparticles have superior transvascular flux into solid tumors: insights from a mathematical model. *Ann. Biomed. Eng.* 41, 68–77 (2013).

75   Park J, Estrada A, Schwartz JA *et al.* Intra-organ biodistribution of gold nanoparticles using intrinsic two-photon-induced photoluminescence. *Lasers Surg. Med.* 42, 630–639 (2010).

76   Vlashi E, Kelderhouse LE, Sturgis JE, Low PS. Effect of folate-targeted nanoparticle size on their rates of penetration into solid tumors. *ACS Nano* 7, 8573–8582 (2013).

77   Smith DM, Simon JK, Baker JRJ. Applications of nanotechnology for immunology. *Nat. Rev. Immunol.* 13, 592–605 (2013).

78   Park YM *et al.* Nanoparticle-based vaccine delivery for cancer immunotherapy. *Immune Network* 13, 177–183 (2013).

79   Mottram PL, Leong D, Crimeen-Irwin B *et al.* Type 1 and 2 immunity following vaccination is influenced by nanoparticle size: formulation of a model vaccine for respiratory syncytial virus. *Mol. Pharm.* 4, 73–84 (2007).

80   Stano A, Nembrini C, Swartz MA, Hubbell JA, Simeoni, E. Nanoparticle size influences the magnitude and quality of mucosal immune respeonse after intranasal immunization. *Vaccine* 30, 7541–7546 (2012).

81   Ahrens ET, Bulte JW. Tracking immune cells *in vivo* using magnetic resonance imaging. *Nat. Rev. Immunol.* 13, 755–763 (2013).

82   Caravan P. Strategies for increasing the sensitivity of gadolinium based MRI contrast agents. *Chem. Soc. Rev.* 35, 512–523 (2006).

83   Larsen EK, Nielsen T, Wittenborn T *et al.* Accumulation of magnetic iron oxide nanoparticles coated with variably sized polyethylene glycol in murine tumors. *Nanoscale* 4, 2352–2361 (2012).

84   Jin Y *et al.* Silica nanoparticles with continuously tunable sizes: synthesis and size effects on cellular contrast imaging. *Chem. Mater.* 20, 4411–4419 (2008).

85   Jain PK, Lee KS, El-Sayed IH, El-Sayed MA. Calculated absorption and scattering properties of gold nanoparticles

of different size, shape, and composition: applications in biological imaging and biomedicine. *J. Phys. Chem. B* 110, 7238–7248 (2006).

86   Link S, El-Sayed MA. Spectral properties and relaxation dynamics of surface plasmon electronic oscillations in gold and silver nanodots and nanorods. *J. Phys. Chem. B* 103, 8410–8426 (1999).

87   Arami H, Ferguson RM, Khandhar AP, Krishnan KM. Size-dependent ferrohydrodynamicrelaxometry of magnetic particle imaging tracers in different environments. *Med. Phys.* 40, 071904 (2013).

88   Ferguson RM, Minard KR, Krishnan KM. Optimization of nanoparticle core size for magnetic particle imaging. *J. Magn. Magn. Mater.* 321, 1548–1551 (2009).

89   Ginzburg VV, Balijepalli, S. Modeling the thermodynamics of the interaction of nanoparticles with cell membranes. *Nano Lett.* 7, 3716–3722 (2007).

90   Li D, Emond C, Johanson G, Jolliet, O. Using a PBPK model to study the influence of different characteristics of nanoparticles on their biodistribution. *J. Phys. Conf. Ser.* 429, 012019 (2013).

•   **Highlights the most current PBPK model and gives examples of future improvements that need to be made.**

91   Frieboes HB, Wu M, Lowengrub J, Decuzzi P, Cristini, V. A Computational model for predicting nanoparticle accumulation in tumor vasculature. *PLoS ONE* 8, e56876 (2013).

92   van de Ven AL, Abdollahi B, Martinez CJ *et al.* Modeling of nanotherapeutics delivery based on tumor perfusion. *New J. Phys.* 15, 055004 (2013).

93   Macklin P, McDougall S, Anderson AR, Chaplain MA, Cristini V, Lowengrub J. Multiscale modelling and nonlinear simulation of vascular tumour growth. *J. Math. Biol.* 58, 765–798 (2009).

94   Wu M, Frieboes HB, Chaplain MA, McDougall SR, Cristini V, Lowengrub JS. The effect of interstitial pressure on therapeutic agent transport: coupling with the tumor blood and lymphatic vascular systems. *J. Theor. Biol.* 355, 194–207 (2014).

95   Godin B, Driessen WH, Proneth B *et al.* An integrated approach for the rational design of nanovectors for biomedical imaging and therapy. *Adv. Genet.* 69, 31–64 (2010).